

Six-Stator Spherical Induction Motor for Balancing Mobile Robots

Ankit Bhatia, Masaaki Kumagai, and Ralph Hollis

Abstract—This paper describes the design, construction, and operation of a closed-loop spherical induction motor (SIM) ball wheel for a balancing mobile robot (ballbot). Following earlier work, this new design has a smaller rotor and higher torques due to the use of six stators in a skewed layout. Actuation and sensing kinematics as well as control methods are presented. In its current implementation, torques of up to 8 Nm are produced by the motor with rise and decay times of 100 ms. Results are presented supporting its potential as a prime mover for mobile robots.

I. INTRODUCTION

It has been nearly a decade since the single spherical wheel balancing mobile robot (ballbot) first appeared [1] (Fig. 1). This qualitatively different locomotion method for mobile robots has been explored and further developed in several laboratories in the U.S., Japan, Australia, and Switzerland. Ballbots are omni-directional, can be as tall and narrow as a person, can have high centers of gravity, and exhibit inherently compliant behavior during collisions or when pushed or shoved by a person. They can move smoothly and gracefully at speeds up to several meters per second, generally exceeding the performance of humanoid robots with a fraction of the cost. Ballbots appear to be particularly suited for interaction with people and operation in everyday human environments.

This work was supported in part by NSF grant ECCS 1102147 and by KAKENHI(23760234) in Japan.

Ankit Bhatia is a Masters Candidate at the Robotics Institute, Carnegie Mellon University, Pittsburgh, PA 15213, USA. ankitbhatia@gmail.com

Masaaki Kumagai is an Associate Professor in the Faculty of Engineering, Tohoku Gakuin University, Tagajo 985-8537 Japan. kumagai@tjcc.tohoku-gakuin.ac.jp

Ralph Hollis is a Research Professor in the Robotics Institute, Carnegie Mellon University, Pittsburgh, PA 15213, USA. rhollis@cs.cmu.edu

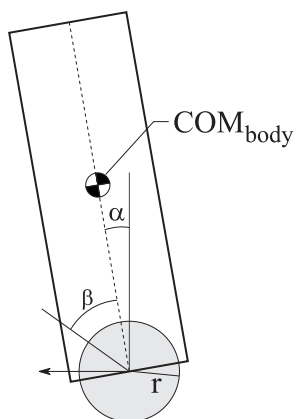


Fig. 1: A ballbot, with lean angle α and ball rotation β .

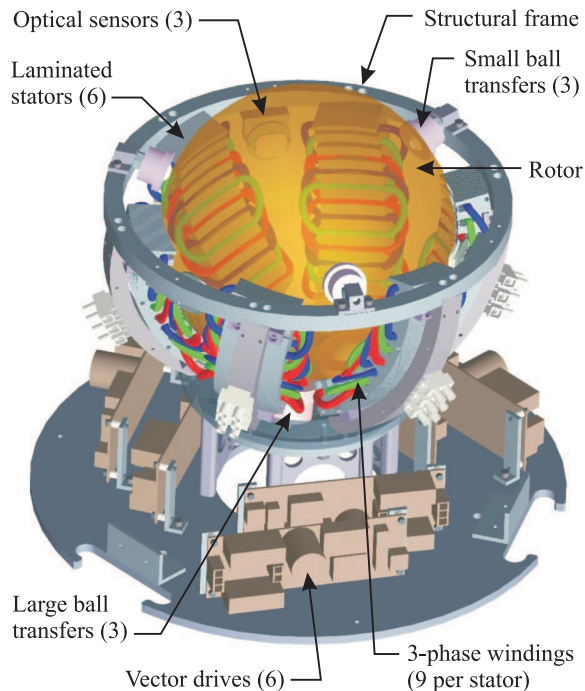


Fig. 2: CAD model of six-stator spherical induction motor (SIM) as a prime mover for ballbots.

Ballbots are potentially very simple machines: there is a body supported by a ball wheel; a key question is “how best to drive the ball?” To date there have principally been two methods. First, there is the “inverse mouse ball (IMB)” [2] wherein four drive motors actuate pairs of orthogonal rollers pressing against the ball to create motion in the plane, while a fifth drive motor provides yaw motion to affect the body azimuth. Second, there is the “tri-wheel” principle [3] wherein three motors drive the ball in all three DOFs using special omni-wheels. Neither of these drive methods is ideal. For example, the IMB inherently has excessive friction whereas the tri-wheel has many complicated small parts and limited load carrying ability. Out of all the possible modes of failure for a ballbot, mechanical failure in the drive mechanism is perhaps the most probable. It therefore seems prudent to investigate a minimal-contact approach for torque generation between the body and ball.

One solution is to replace the current mechanical drive mechanisms with some form of continuous rotation spherical motor, thereby reducing the number of moving parts in the robot to just the ball and the body which would in turn, markedly reduce the probability of mechanical failure.

Previously, many different ideas for spherical actuators



Fig. 3: Photo of as-built six-stator spherical induction motor.

have been investigated using ultrasonic [4] or electromagnetic actuation [5], [6], but fall short of being a suitable candidate for a prime mover due to either low power output, limited range of motion or a complex rotor design. Two of the authors have previously investigated the development and control of a spherical induction motor (SIM) with potential characteristics of a prime mover for mobile robots [7]. Induction drives are suitable for such a motor as a consequence of relatively simple rotor construction, the lack of mechanical commutation and reliability. This paper extends the work described above and reports the first design, implementation, and control of a new higher torque six stator spherical induction motor specifically for use in ballbots.

II. MOTOR DESIGN

A SIM, like any induction motor, has a rotating and a stationary component referred to as the rotor and the stator respectively. In the design shown in Fig. 2, six stators are mounted in a skewed configuration on a strong structural frame made with 7075-T6 Aluminum alloy to resist attractive forces produced between the stators and the rotor. The frame also has mounting points for motion sensors and other electronics, and nylon ball transfers needed to support the rotor and maintain a fixed air gap.

For a ballbot, large ball torques in roll and pitch are needed for balancing and moving about on the floor whereas a smaller torque in yaw output is acceptable for orienting the body to face a particular direction. These considerations dictate the present design. The SIM described here has six stators centered 40° north of the equatorial

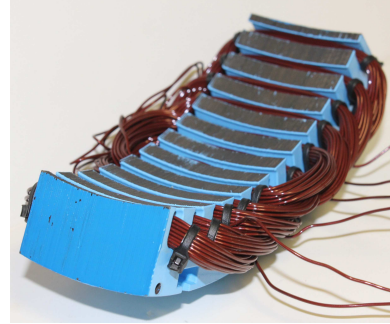


Fig. 4: Photo of one of the six stators with windings in place.

plane of the rotor with each stator skewed 10° from the rotor's polar axis. Given that the rotor must support all of the weight of the robot, a key design criteria required the rotor to be strong and rigid.

A. Rotor design and construction

The rotor has a hollow soft steel core and an outer copper shell. To manufacture the rotor, two hollow hemispheres 6.35 mm thick were first fabricated from a solid billet of SAE 1018 alloy steel, followed by annealing. These hemispheres were then oven brazed together and electroplated with 60/40 Pb/Sn solder. The outer copper hemispherical shells were produced by a spinning process followed by machining to a thickness of approximately 1.3 mm. They were then electroplated on the insides with solder. The core and copper hemispheres were joined together by shrink-fitting, that is, the copper hemispheres were heated (expansion) and the core was cooled (contraction) and then the three parts were forced together in a specially built press. The assembled rotor was then heated above the melting point of the solder to permanently bond them together and to insure electrical conductivity across the two copper shells. As a final step the rotor was ground in a centerless spherical grinding machine and lapped to an outer diameter of 202.7 ± 0.25 mm.

B. Stator design and construction

An individual stator, shown in Fig. 4, is a force producing unit in the SIM. There are a total of 6 stators, combinations of which can produce any torque within the actuation envelope. With the current vector drive electronics (see [7]), each stator can produce approximately 40 N of continuous tangential force on the rotor with a 70 N peak force for less than 0.5 s. The stators are made of 72 M19 electrical steel laminations with C5 insulation which were laser cut and then stress relieved annealed. Each stator stack has two half stacks of 36 laminations each which when aligned, stacked, and bonded form a spherical surface with a uniform air gap of approximately 1 mm from the rotor. The stacks were bonded with 3M ScotchcastTM and powder coated in a fluidized bed for insulation and to prevent the sharp edges from damaging the windings. The stators have 12 slots which are wound with 9 coils to create

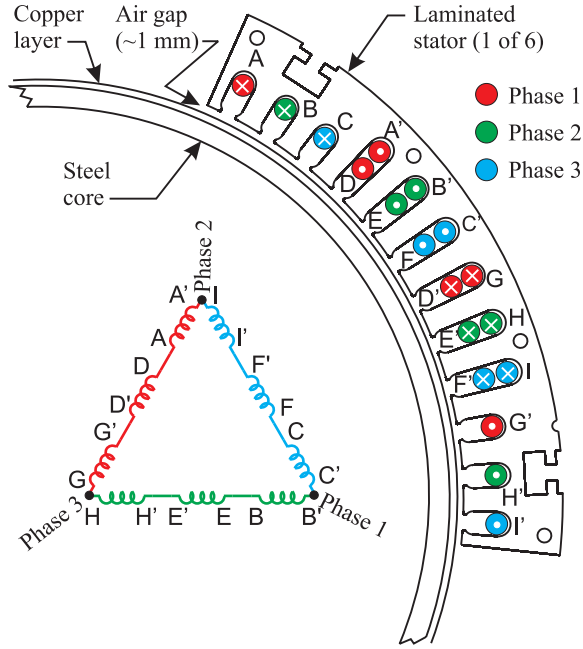


Fig. 5: Schematic drawing of the stator-rotor interface showing the three phases and delta winding scheme.

TABLE I: SIM Parameters

Parameter	Symbol	Value
Ball radius	r_b	0.1013 ± 0.00012 m
Ball inertia	I_b	0.050 Kg m ²
Ball mass	m_b	7.46 Kg
Copper shell thickness	d_{Cu}	0.0013 m
Steel core thickness	d_{Fe}	0.0625 m
Roller static friction	f_s	0.4 Nm

a 3-phase 4-pole arrangement. Each coil is wound with 25 turns of AWG 19 double polyimide insulated wire rated to 300°C. Coil resistance R and inductance L is 0.37 Ohm and 1.03 mH measured at 50 Hz, giving an electrical time constant of $L/R = 3.5$ ms. Figure 5 shows the arrangement of the coils on a single stator which are driven by 3 phases separated by 120° in a delta configuration. The excitation causes a moving magnetic field traveling along the length of the stator generating currents in the copper layer that drags the rotor in the same direction as the moving field. Principle characteristics of the as-built SIM are shown in Table I.

III. ACTUATION KINEMATICS

In combination, the six stators surrounding the rotor provide any three dimensional torque. The traction forces from each of these six stators can be averaged to a linear force applied tangential to the rotor at a point on the rotor adjacent to the center of the stator. The action of one such stator is shown in Figure 6. The force is assumed to be applied at a point \mathbf{p}_i described by spherical coordinates r , θ and ϕ where r_b is the radius of the rotor. The average force is applied in the direction \mathbf{f}_i which is tangential to

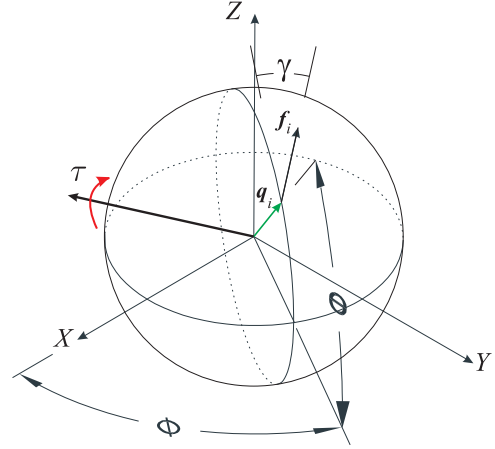


Fig. 6: The action of force generated from a single stator is assumed to act at a point on the rotor tangential to the surface to produce the torque τ .

the sphere and skewed by an angle γ from the great circle. The vectors \mathbf{q}_i and \mathbf{f}_i are given by

$$\mathbf{q}_i = \begin{bmatrix} r_b \cos \theta \cos \phi \\ r_b \cos \theta \sin \phi \\ r_b \sin \theta \end{bmatrix}, \quad (1)$$

$$\mathbf{f}_i = \begin{bmatrix} -\sin \gamma \sin \phi - \cos \gamma \sin \theta \cos \phi \\ \sin \gamma \cos \phi - \cos \gamma \sin \theta \sin \phi \\ \cos \gamma \cos \theta \end{bmatrix}. \quad (2)$$

For the design described in the paper, $\theta = 40^\circ$, $\gamma = 10^\circ$ and ϕ ranges from 0 to 360° in steps of 60°.

The relation between torque generated and force commanded is the cross product between \mathbf{q}_i and \mathbf{f}_i which can be arranged in the columns of the matrix M_a ,

$$M_a = [p_1 \times \hat{s}_1 \quad \dots \quad p_6 \times \hat{s}_6], \quad (3)$$

where $\hat{s}_1, \dots, \hat{s}_6$ are unit vectors associated with each stator such that

$$\begin{bmatrix} F_1 \\ \vdots \\ F_6 \end{bmatrix} = M_a^+ \begin{bmatrix} \tau_x \\ \tau_y \\ \tau_z \end{bmatrix}, \quad M_a^+ = M_a^T (M_a^T M_a)^{-1}. \quad (4)$$

Here, the operation M_a^+ signifies the pseudo inverse. Using the pseudo inverse ensures an optimal set of forces for a particular torque for this over-actuated design. For the set of coordinates specified above, the actuation matrix is given by

$$M_a^+ = \begin{pmatrix} -0.3788 & -3.342 & 12.53 \\ 2.705 & -1.999 & 12.53 \\ 3.083 & 1.343 & 12.53 \\ 0.3788 & 3.342 & 12.53 \\ -2.705 & 1.999 & 12.53 \\ -3.083 & -1.343 & 12.53 \end{pmatrix}. \quad (5)$$

The particular arrangement of six stators results in a polyhedral volume in torque space as shown in Fig. 7. As

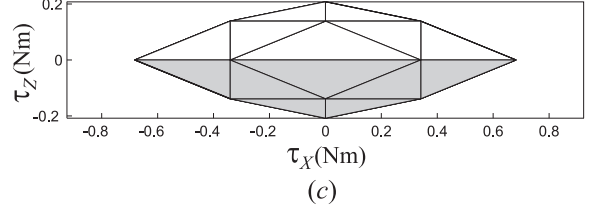
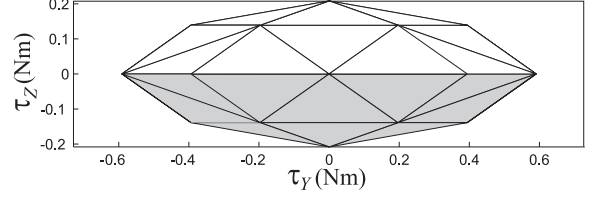
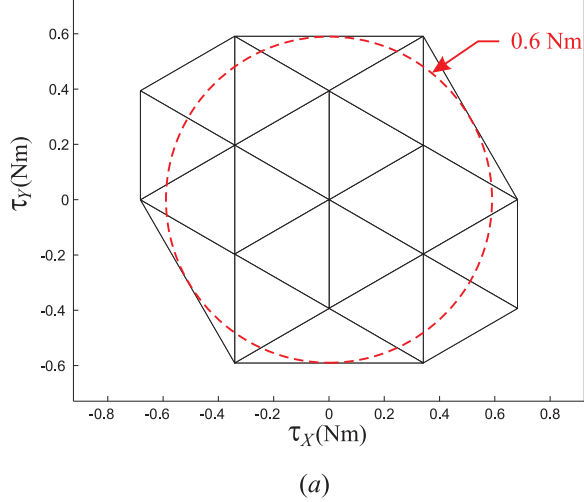


Fig. 7: Motor torque actuation space for a unit force produced by stators in the (a) XY plane, (b) YZ plane, and (c) ZX plane.

previously noted, actuation is biased in favor of the XY (pitch, roll) plane. The inscribed circle in Fig. 7(a) denotes the isotropic force range at $\tau_z = 0$ (zero yaw torque).

IV. SENSING KINEMATICS

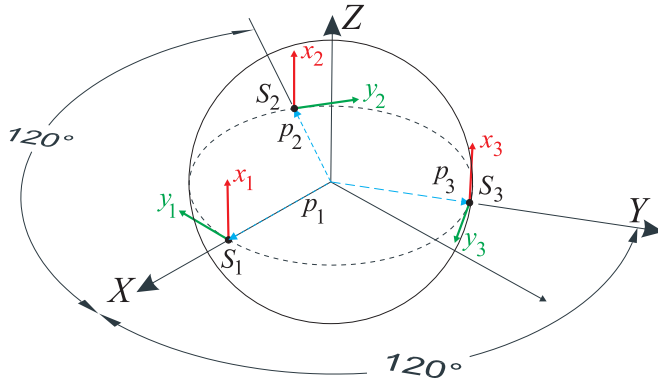


Fig. 8: Vectors describing measured surface velocities at each laser mouse sensor.

For closed loop operation, one must measure the angular position and velocity of the rotor. For this task, optical laser mouse sensors (Avago ADNS-9800) track scratches on the ball and provide displacements. Tracking the orientation of the rotor relies on 6 surface velocity measurements from 3 laser mouse sensors, similar to that of [7]. Figure 8 shows the vectors \mathbf{p}_i to the location of each of the sensors s_i and their sensing directions x_i and y_i , $i = 1, \dots, 3$. The sensors are arranged at 120° intervals in the rotor's equatorial plane. The following relation maps the angular velocity of the ball to the surface velocities v_{x_i} ,

v_{y_i} .

$$\begin{bmatrix} \omega_x \\ \omega_y \\ \omega_z \end{bmatrix} = M_s^+ \begin{bmatrix} v_{x_1} \\ v_{y_1} \\ \vdots \\ v_{x_3} \\ v_{y_3} \end{bmatrix}, M_s^+ = (M_s^T M_s)^{-1} M_s^T, \quad (6)$$

where

$$M_s = \begin{bmatrix} (\mathbf{p}_1 \times \hat{\mathbf{v}}_{x_1})^T \\ (\mathbf{p}_1 \times \hat{\mathbf{v}}_{y_1})^T \\ \vdots \\ (\mathbf{p}_3 \times \hat{\mathbf{v}}_{x_3})^T \\ (\mathbf{p}_3 \times \hat{\mathbf{v}}_{y_3})^T \end{bmatrix}. \quad (7)$$

Referring to Fig. 8,

$$\mathbf{p}_1 = \begin{bmatrix} 1 \\ 0 \\ 0 \end{bmatrix}, \mathbf{p}_2 = \begin{bmatrix} -\cos 60^\circ \\ \sin 60^\circ \\ 0 \end{bmatrix}, \mathbf{p}_3 = \begin{bmatrix} -\cos 60^\circ \\ -\sin 60^\circ \\ 0 \end{bmatrix}. \quad (8)$$

$$\mathbf{x}_1 = \begin{bmatrix} 0 \\ 0 \\ 1 \end{bmatrix}, \mathbf{y}_1 = \begin{bmatrix} 0 \\ -1 \\ 0 \end{bmatrix}, \mathbf{y}_2 = \begin{bmatrix} \cos 30^\circ \\ \sin 30^\circ \\ 0 \end{bmatrix}, \mathbf{y}_3 = \begin{bmatrix} -\cos 30^\circ \\ \sin 30^\circ \\ 0 \end{bmatrix}. \quad (9)$$

Using the calculated vectors and Eqs. 6 and 7 the sensor matrix is given by

$$M_s = \begin{pmatrix} 0 & 0 & -0.1 \\ 0 & -0.1 & 0 \\ 0 & 0 & 0.05 \\ 0.0866 & 0.05 & 0 \\ 0 & 0 & 0.05 \\ -0.0866 & 0.05 & 0 \end{pmatrix}. \quad (10)$$

The rotor angular pose is calculated by ordered integration of the angular velocities ω_x , ω_y , and ω_z .

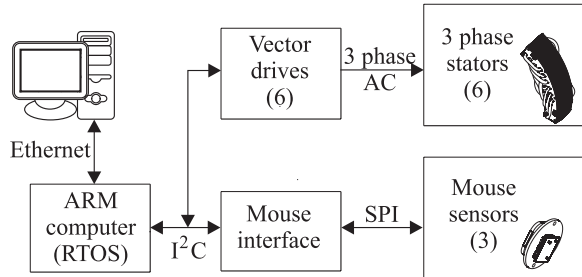


Fig. 9: System Architecture for the spherical induction motor.

A. System Architecture

Figure 9 shows the distributed system architecture for the SIM. Different subsystems are interconnected over an I²C bus [8]. The master controller on the bus is a RISC based ARM microcontroller running at 1 GHz. This microcontroller is tasked with running the closed loop higher level velocity or orientation controllers and communicating with the other devices on the bus to write force commands or read velocity data.

The stator vector drives and mouse interfaces connected to the I²C bus and SPI bus are responsible for closed loop current control and sensor velocity reporting respectively. Each transaction, including writing to all six vector drives and reading the 3 mouse sensors takes less than 1.5 ms allowing higher level closed loop control at up to 500 Hz.

B. Sensorless Field Oriented Control

In rotary AC induction motors, 3 phase line voltages are used to generate torque. Generally, the voltage and frequency applied are calculated based on motor parameters, target speed and applied load. Since these motors are normally designed for steady state, these methods are less efficient for servo control. The SIM therefore uses a field-oriented controller (vector drive) which closes the loop on current at 10 KHz at each stator to control torque allowing better transient characteristics and faster response times. Details of the vector drives currently used in the SIM can be found in [9].

The aim of a sensorless field oriented controller is to decouple the magnetizing current i_d and force-producing current i_q . The currents i_d and i_q are along the principal axes in a rotating frame where ϕ is the angle between the stationary and rotating frames. Two PI control loops individually control i_d and i_q while an observer estimates ϕ based on the measured currents in the three windings [10]. The force produced in the stator depends directly on the product of i_d and i_q ,

$$F \propto i_d i_q, \quad (11)$$

and the resultant current I in the windings is given by

$$I = \sqrt{i_d^2 + i_q^2}. \quad (12)$$

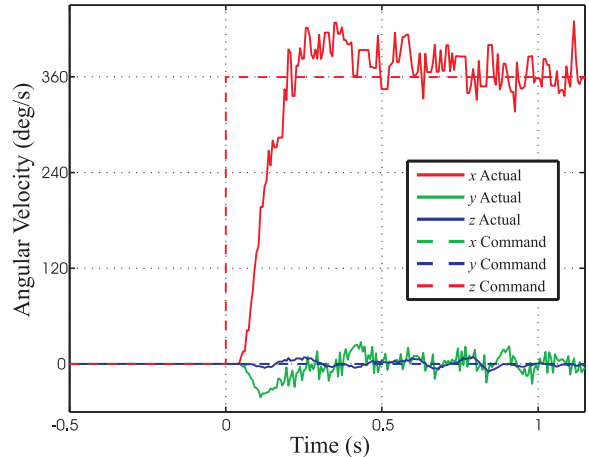


Fig. 10: Response to step command in angular velocity.

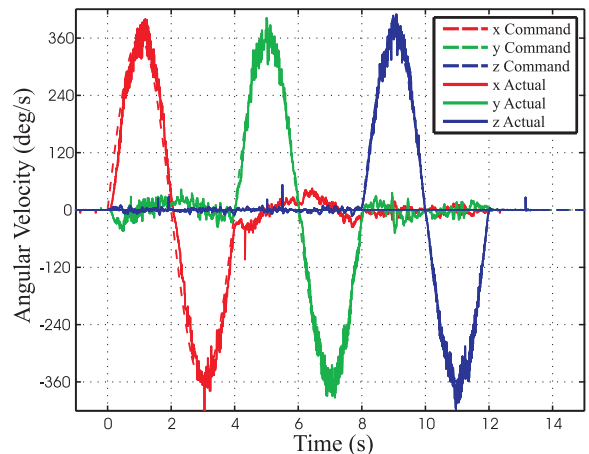


Fig. 11: Successive rotations about all three axes commanded by sine waves.

V. CONTROL METHOD

A PID control scheme is used for angular velocity control of the ball. In previous sections, a method for open loop torque generation and angular velocity measurement is shown. Given a desired angular velocity $\vec{\omega}_d$ and a measured angular velocity, $\vec{\omega}$ the velocity error $e_{velocity}$ is defined as

$$e_{velocity} = \vec{\omega}_d - \vec{\omega}. \quad (13)$$

The torque command can be calculated based on the PID control law

$$\vec{\tau} = K_p e + K_d \dot{e} + K_i \int e dt. \quad (14)$$

VI. RESULTS

We have tested the new SIM using several simple control methods. Figure 10 shows the x-axis velocity step response going from 0 to 1 rev/s in approximately 0.2 s. Figure 11 shows velocities for successive rotations about the x, y, and z axes. Figure 12 is the x-axis response to a step current command, showing rise and decay times of

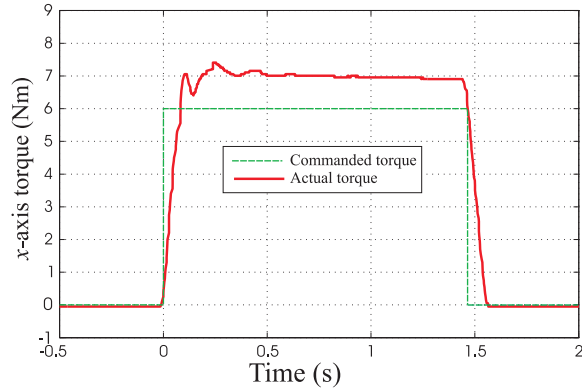


Fig. 12: Locked rotor response to step in torque control.

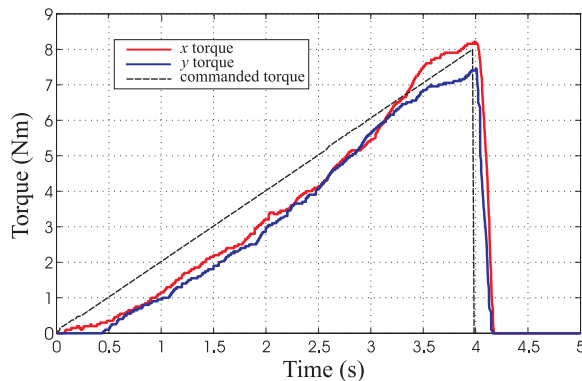


Fig. 13: Actual vs. commanded torque around x and y axes.

approximately 100 ms. Figure 13 shows the x- and y-axis torque response to an input ramp. Here, there is some lag due partly to static friction in the ball transfers as well as system timing delays. Currently, peak torques are limited to approximately 8 Nm due to limitations of the vector drives. Erroneous sensor readings were noted to occur at the rate of a few times per second, presumably due to the PWM waveforms in the nearby windings. These data points were rejected by a simple filtering scheme and are likely to be eliminated with additional attention paid to shielding and grounding.

VII. CONCLUSION

Unlike previous work [7], the SIM described in this paper has been designed to serve as the drive unit for a ballbot. In normal operation, the 51 Kg IMB-based ballbot [2] operates with lean angles α bounded between $-5^\circ < \alpha < 5^\circ$ (see Fig. 1). This ballbot model was simulated with the SIM substituting for the IMB. Figure 14 shows the response required to stabilize from a 5° initial lean without falling. The peak torque was clamped to be within ± 8 Nm. It is known that the IMB ballbot referred to above can generate up to ± 40 Nm using four conventional dc motors. On the other hand, when comparing static friction characteristics, the SIM has only 0.4 Nm of friction whereas the IMB has 3.6 Nm. As noted above,

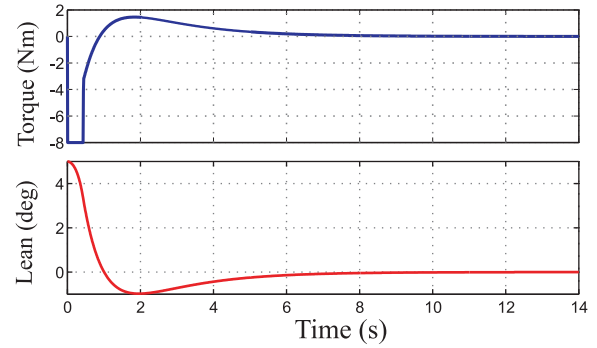


Fig. 14: Simulated response of a 51 Kg SIM-based ballbot model successfully recovering from an initial 5° lean angle.

we are presently limited by the capacities of the vector drives. Operation is well below magnetic saturation levels as evidenced by the torque curves seen in Fig. 13. A successful SIM would enable the creation of a very simple high-performance mobile robot: a mechanically minimal “SIMbot” with only a body and a ball. Other applications in multi-wheeled robots or omni-directional freight handling systems might be possible.

VIII. FUTURE WORK

Much work remains to fully characterize the as-built SIM, including the completion of higher power vector drives. Various traction coatings or hard plating on the rotor will serve to increase ruggedness when used as a wheel. The ball transfers could be replaced with air bearings to eliminate static friction.

REFERENCES

- [1] T. Lauwers, G. Kantor, and R. Hollis, “One is enough!” in *Proc. Int’l. Symp. for Robotics Research*. San Francisco: Int’l. Foundation for Robotics Research, October 12-15 2005.
- [2] U. Nagarajan, G. Kantor, and R. Hollis, “The ballbot: An omnidirectional balancing mobile robot,” *Int’l J. of Robotics Research (IJRR)*, vol. 33, no. 6, pp. 917–930, May 2014.
- [3] M. Kumagai and T. Ochiai, “Development of a robot balancing on a ball,” *International Conference on Control, Automation and Systems*, 2008.
- [4] S. Toyama, S. Sugitani, Z. Guoqiang, Y. Miyatani, and K. Nakamura, “Multi degree of freedom spherical ultrasonic motor,” in *Robotics and Automation, 1995. Proceedings., 1995 IEEE International Conference on*, vol. 3. IEEE, 1995, pp. 2935–2940.
- [5] K. Kaneko, I. Yamada, and K. Itao, “A spherical dc servo motor with three degrees of freedom,” *Journal of dynamic systems, measurement, and control*, vol. 111, no. 3, pp. 398–402, 1989.
- [6] K.-M. Lee, H. Son, J. Joni et al., “Concept development and design of a spherical wheel motor (SWM),” in *IEEE International Conference on Robotics and Automation*, vol. 4. IEEE; 1999, 2005, p. 3652.
- [7] M. Kumagai and R. Hollis, “Development and control of a three DOF spherical induction motor,” in *IEEE Int’l. Conf. on Robotics and Automation*, Karlsruhe, Germany, May 6-10 2013.
- [8] P. Semiconductors, “The I²C bus specification,” *Philips Semiconductors*, vol. 9397, no. 750, p. 00954, 2000.
- [9] M. Kumagai and R. Hollis, “Development and control of a three DOF planar induction motor,” in *IEEE Int’l. Conf. on Robotics and Automation*, St. Paul, MN, May 14-18 2012.
- [10] M. Kumagai, “Development of a linear induction motor and a vector control driver,” in *SICE Tohoku chapter workshop material*, 2010, pp. 262–9.